Telomeres stall DNA loop extrusion by condensin

Analikwu, Brian T.; Deshayes, Alice; van der Torre, Jaco; Guérin, Thomas M.; Katan, Allard J.; Barth, Roman; Mattarocci, Stefano; Dekker, Cees; Marcand, Stéphane; More Authors

DOI
10.1016/j.celrep.2025.115900

Publication date
2025

Document Version
Final published version

Published in
Cell Reports

Cell Reports

Telomeres stall DNA loop extrusion by condensin

Graphical abstract

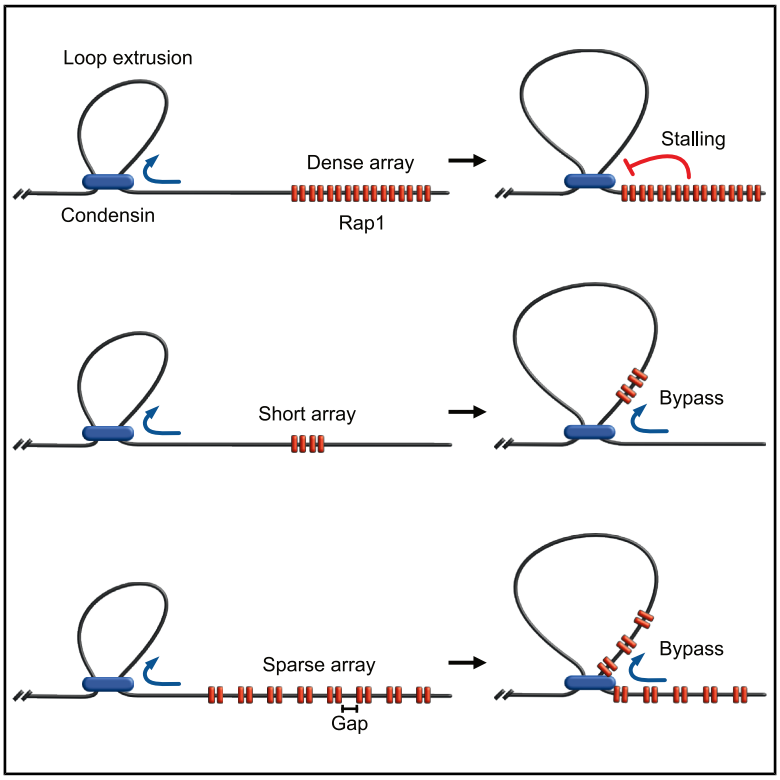

Highlights

- Dense linear Rap1 arrays on DNA halt DNA loop extrusion by condensin
- The blocking efficiency depends on array length and DNA gap size
- Rap1 accumulates condensin and decompacts chromatin in anaphase

Authors

Brian T. Analikwu, Alice Deshayes, Jaco van der Torre, ..., Stefano Mattarocci, Cees Dekker, Stéphane Marcand

Correspondence

stefano.mattarocci@inserm.fr (S.M.), c.dekker@tudelft.nl (C.D.), stephane.marcand@cea.fr (S.M.)

In brief

Analikwu et al. show that dense linear arrays of the telomeric protein Rap1 on DNA block DNA loop extrusion by condensin. Rap1-induced stalling depends on array length and protein density and leads to a local chromatin decompaction during anaphase, revealing how protein arrays can regulate SMC-driven genome organization.

Analikwu et al., 2025, Cell Reports *44*, 115900
July 22, 2025
https://doi.org/10.1016/j.celrep.2025.115900

CellPress

Cell Reports

CellPress
OPEN ACCESS

Report

Telomeres stall DNA loop extrusion by condensin

Brian T. Analikwu,[1,4] Alice Deshayes,[2,4] Jaco van der Torre,[1] Thomas M. Guérin,[2] Allard J. Katan,[1] Claire Béneut,[2] Roman Barth,[1] Jamie Phipps,[2] Vittore Scolari,[3] Xavier Veaute,[2] Didier Busso,[2] Karine Dubrana,[2] Stefano Mattarocci,[2,*] Cees Dekker,[1,*] and Stéphane Marcand[2,5,*]

[1]Kavli Institute of Nanoscience Delft, Delft University of Technology, Delft, the Netherlands
[2]Université Paris-Saclay, Université Paris-Cité, CEA, Inserm, Institut de Biologie François Jacob, UMR Stabilité Génétique Cellules Souches et Radiations, Fontenay-aux-Roses, France
[3]Institut Curie, PSL Research University, Sorbonne Université, Paris, France
[4]These authors contributed equally
[5]Lead contact
*Correspondence: stefano.mattarocci@inserm.fr (S.M.), c.dekker@tudelft.nl (C.D.), stephane.marcand@cea.fr (S.M.)
https://doi.org/10.1016/j.celrep.2025.115900

SUMMARY

DNA loop extrusion by SMC proteins is a key process underlying chromosomal organization. It is unknown how loop extruders interact with telomeres where DNA is densely covered with proteins. Using complementary *in vivo* and *in vitro* single-molecule approaches, we study how loop-extruding condensin interacts with Rap1, the telomeric DNA-binding protein of *Saccharomyces cerevisiae*. We show that dense linear Rap1 arrays can completely halt DNA loop extrusion, with a blocking efficiency depending on the array length and the DNA gap size between proteins. In anaphase cells, dense Rap1 arrays are found to accumulate condensin and to cause a local chromatin decompaction, as monitored with a microscopy-based approach, with direct implications for the resolution of dicentric chromosomes produced by telomere fusions. Our findings show that linear arrays of DNA-bound proteins can efficiently halt DNA loop extrusion by SMC proteins, which may impact cellular processes from telomere functions to transcription and DNA repair.

INTRODUCTION

Telomeres are essential protein-DNA complexes that prevent chromosome ends from being mistaken for DNA breaks. They consist of long stretches of short repeated motifs, tightly covered by sequence-specific DNA-binding proteins like Rap1 in budding yeast.[1–4] This tight packing restricts access to telomere DNA for processes such as transcription, repair, and replication.[5–12]

Here, we explore how such tight DNA coverage is handled by a key chromosomal organizer, the SMC complex (Structural Maintenance of Chromosomes) condensin. SMC complexes are motor proteins that extrude DNA loops to organize chromatin into higher-order structures.[13–20] Condensin compacts chromosomes during mitosis via loop extrusion[21–25] and is essential to segregation.[26,27] Condensin consists of two ATPase SMC subunits (Smc2, Smc4), a kleisin (Brn1), and two HEAT-repeat subunits (Ycs4 and Ycg1). Yeast condensin acts as a monomer, anchoring DNA at the Brn1-Ycg1 interface and extruding loops from that point.[15,18,28,29] This activity is driven by ATP-dependent conformational changes and dynamic DNA-protein contacts.[18,30–33]

It is currently intensely studied whether condensin and other SMC complexes are blocked by DNA-binding proteins acting as roadblocks.[34–38] CTCF, which demarcates topologically associated domains,[36,39] was recently shown to block cohesin in a direction- and force-dependent manner through specific chemical interactions.[35] In contrast, SMC complexes can bypass isolated physical roadblocks on DNA *in vitro* in the absence of specific interactions.[38,40] However, cellular chromosome-bound roadblocks are often denser and not isolated. For instance, RNA polymerases may stall SMC complexes at highly transcribed genes, perhaps due to DNA coverage by "polymerase trains."[34,41–47]

Our previous work suggested that condensin may stall at telomeres.[12] Upon studying dicentric chromosome breakage in *Saccharomyces cerevisiae*, we found that dicentrics from accidental telomere-telomere fusions preferentially broke at the fusion points[48] during abscission (septum closure in yeast).[12,49,50] This restored the parental karyotype, offering a backup pathway for telomere protection. Breakage at telomere fusions requires two specific actors, condensin and the telomere DNA-binding protein Rap1. Condensin stalling by Rap1 arrays might favor their capture at abscission sites, explaining the preferential breakage at fusion points.[12]

Here, we combine *in vitro* single-molecule and *in vivo* approaches to directly address how Rap1 arrays impact condensin-driven loop extrusion. Dense, tightly bound telomeric repeats provide a unique setting to study this interaction mechanistically. We show that exogenous insertion of Rap1 arrays into chromosomes causes local condensin accumulation and chromatin decompaction. Single-molecule visualizations of individual loop-extruding condensin complexes encountering Rap1 arrays showed that ~100-nm arrays can stall loop extrusion by physical blockage with near-100% efficiency. Stalling depends on DNA

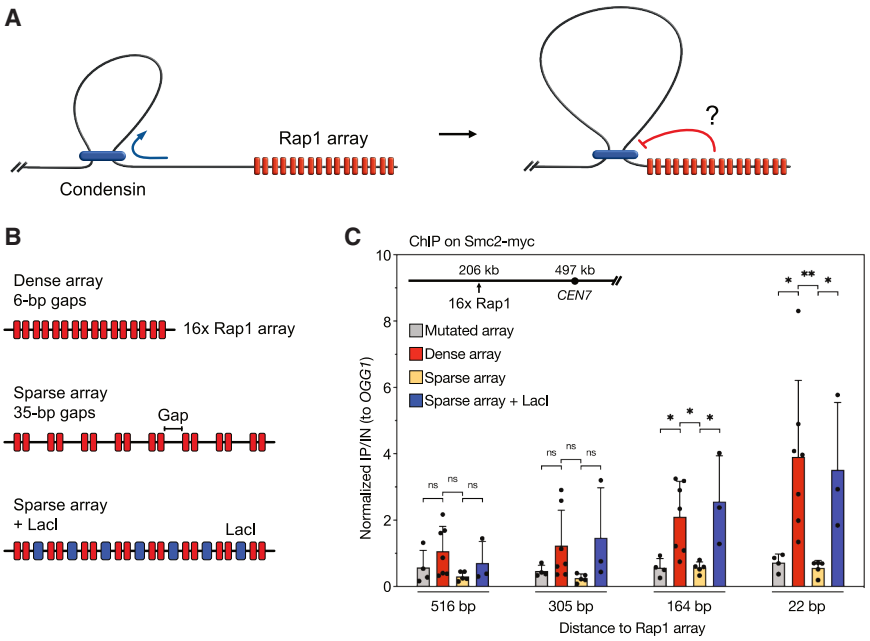

Figure 1. Condensin enrichment at the border of Rap1-bound arrays

(A) Hypothesis for condensin stalling at Rap1-bound arrays.

(B) Scheme of Rap1 arrays used in this study. Tandem repeats contain two consecutive Rap1 binding sites separated by gaps of controlled size. Arrays with 35-bp gaps contain a LacO sequence that LacI protein can bind.

(C) ChIP of Smc2-Myc in cells synchronized in late anaphase. Bars show mean IP/Input values normalized to an ectopic control; error bars indicate standard deviation from ≥3 biological replicates. Statistical significance is from unpaired t test. Unnormalized values in Figure S1.

tension and protein density – small intra-array gaps sharply decrease blocking. These results (1) deepen our mechanistic understanding of DNA loop extrusion, demonstrating that linear protein arrays can block it with unprecedented efficiency; (2) support the hypothesis that telomere-telomere fusions break at fusion points due to force focusing via Rap1-mediated condensin stalling; (3) uncover a new feature of telomeres; and (4) highlight the intricate interplay between SMC-driven structure, DNA stiffness, and protein occupancy.

RESULTS

Condensin is enriched at Rap1 arrays

Stalling of condensin-driven DNA loop extrusion at dense telomere Rap1 arrays could lead to local condensin accumulation at array edges (Figure 1A). To test this hypothesis, we engineered Rap1 binding-site arrays mimicking native telomere length and density[12,51] into the genome. These arrays contained 16 Rap1 sites arranged as pairs (1 bp apart) separated by constant gaps of either 6 or 35 bp (Figure 1B; STAR Methods). Subsequently, we used chromatin immunoprecipitation (ChIP) to map condensin-DNA interactions near these arrays (Figures 1C and S1). To maximize condensin encounters with Rap1-bound arrays, cells were crosslinked in late anaphase (30 min after release from a *cdc15-2*^{ts} arrest),[12,22,50] when condensin-dependent chromosome-arm compaction peaks.[22]

We observed that a dense array of 16 closely spaced Rap1 sites (6-bp gaps) led to a 5-fold increase in condensin at the array border, compared to an array made of mutated DNA sites that are incapable of binding Rap1[12] (Figure 1C). Condensin accumulation decreased with distance from the array, indicating that the accumulation was localized at the edge of the Rap1 array. We saw a similar enrichment at a native telomere (Figure S2), consistent with reports of condensin enrichment at telomeres during mitosis in yeast and vertebrates.[52–54]

If condensin enrichment resulted from condensin stalling at the Rap1 array, then reducing Rap1 density might alleviate it, for example, by exposing bare DNA segments within the array that condensin could contact during the process of loop extrusion. To investigate this, we tested an array of 16 Rap1 sites that were spaced with a 35-bp bare DNA linker between every two successive sites (Figure 1B). Since Rap1 binds uncooperatively,[55] spacing should reduce density without affecting affinity.[55] As anticipated, lower Rap1 density strongly reduced condensin accumulation at the border of the array (Figure 1C). Because the sparse arrays are longer than the dense arrays, stalling appears to be primarily due to the high local density of proteins rather than the length of the array.

To assess whether stalling arises from a purely physical blockade, as opposed to possible chemical interactions, we engineered the 35-bp linkers to contain *LacO* sites, allowing LacI to fill the gaps between the Rap1 proteins. Notably, LacI and Rap1 bind their respective site with similar affinities.[55–57] Expressing LacI dimers in cells harboring these 35-bp linkers restored condensin accumulation to levels seen with the 6-bp spaced dense array (Figure 1C). Condensin was also enriched at tandem arrays of LacI-bound *lacO* sites (Figure S3). These findings indicate that the stalling of DNA loop extrusion by condensin can be attributed to mere physical interactions, rather than due to chemical interactions with Rap1.

High-density Rap1 arrays stall loop extrusion *in vitro*

Previous *in vitro* experiments showed that, surprisingly, most single DNA-binding proteins pose little barrier to loop-extruding condensin.[38] Condensin can even pass 200-nm DNA-bound beads—larger than its ring size—and accommodate those into the extruded loop.[38] Here, we used the same single-molecule-visualization assay to test whether high-density Rap1 arrays alone block loop extrusion. We inserted a Rap1 array into a long (42-kb) DNA molecule, incubated the construct with purified fluorescently labeled Rap1 at a 5× to 7× excess relative to the number of binding sites. Then, Rap1-bound DNA was flushed into a

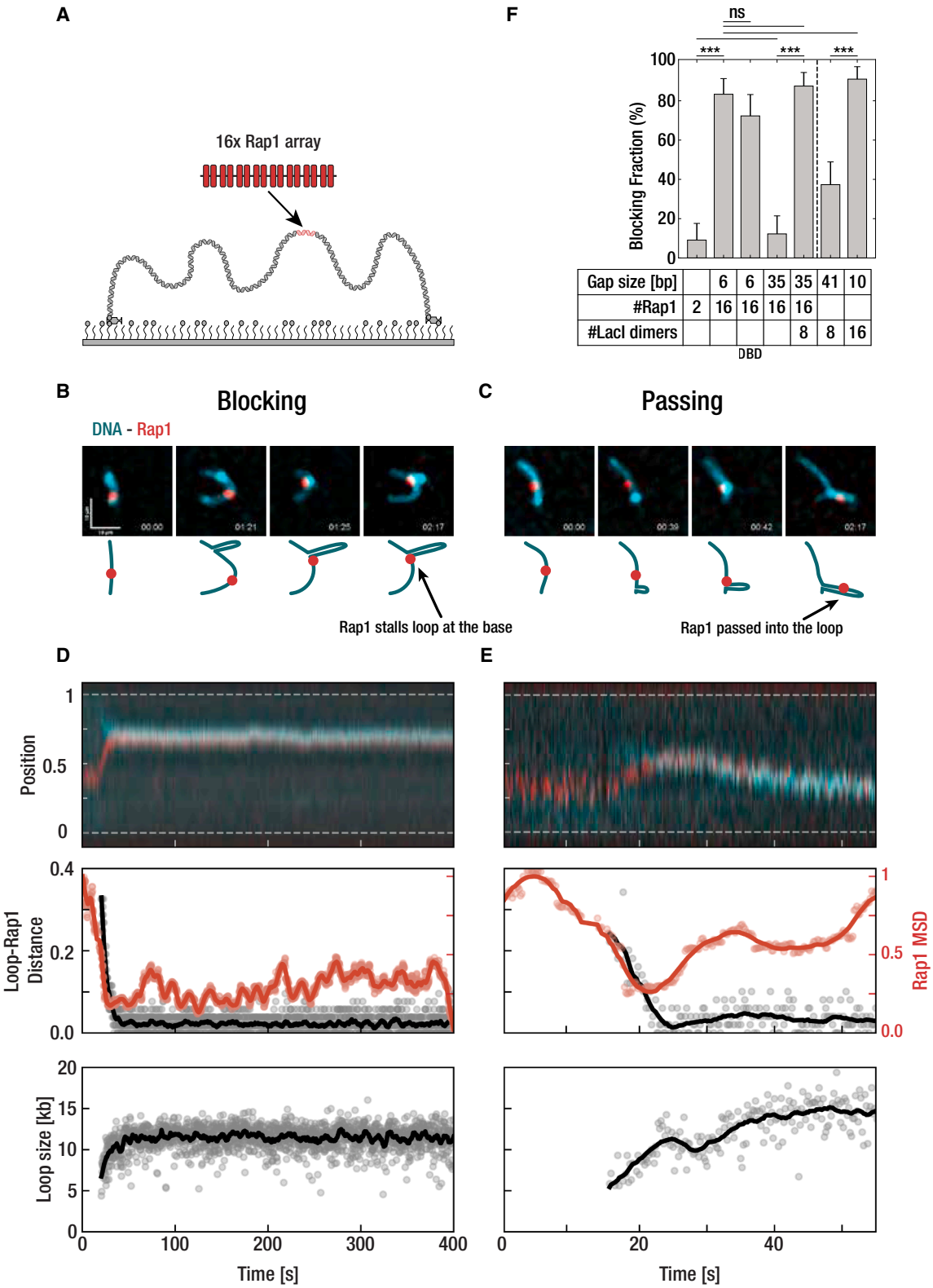

(legend on next page)

flow channel with a pegylated and biotinylated surface to which the biotinylated ends of the DNA molecules attached via biotin-streptavidin binding (Figure 2A). DNA was visualized with the fluorescent intercalator Sytox Orange, which had minimal effect on loop extrusion (Figure S4). We verified that loop extrusion also occurs without intercalator, using DNA labeled with a covalently attached fluorophore (Figure S4C). We also verified that condensin did not stall at the engineered Rap1 array in the absence of Rap1 protein (Figure S4D). Rap1 bound efficiently and specifically to its binding site under these conditions, with near-100% binding efficiency and negligible off-target binding (Figures S5A–S5C; STAR Methods), consistent with its high affinity *in vitro* ($K_D \approx$ 3 nM).[55,57,58] Rap1 residence time, measured under our imaging conditions (Figures S5D–S5G; STAR Methods), showed binding far exceeding the acquisition time for loop extrusion experiments (median residence time 166 min, compared to <30 min acquisition time). From these data we concluded that our linear Rap1 arrays were saturated with bound Rap1 proteins during the single-molecule experiments.

After binding our Rap1 protein arrays in the flow cells, we added condensin (see STAR Methods) to observe encounters between the arrays and loop-extruding condensin. High-density linear Rap1 arrays (16 Rap1 binding sites with 6-bp gap, as used *in vivo*) clearly stalled loop extrusion. This was first visualized qualitatively under buffer flow applied perpendicular to the direction in which DNA was inserted. Figure 2B shows a typical blocking event: a DNA loop (cyan) developed and was stalled upon reaching the Rap1 array (red); Figure 2C shows a passing event, where condensin bypassed the array and accommodated that into the extruded loop. To quantify blocking without flow-associated force, imaging was performed after buffer flow was stopped. Analysis on resulting kymographs (fluorescent intensity along DNA over time) was performed as previously described.[20] We defined stalling as an event that displayed a vanishingly small distance between the Rap1 array and the loop, along with a plateau in both loop size and moving mean squared displacement (MSD) (see STAR Methods and Pradhan et al.[38]). By contrast, passing events showed continued loop growth and raising moving MSD upon encounter (cf. Figures 2B and 2C for kymograph analysis). Blocking efficiency was then calculated as the fraction of stalling events out of total encounters.

High-density linear Rap1 arrays with 16 consecutively bound proteins efficiently stalled loop extrusion, with a blocking efficiency of 83% ± 8% (N = 84) (Figure 2F). This is higher than has been measured for any other DNA-binding protein[38] and exceeds blocking by cohesin-CTCF interactions involving chemical specificity.[35] In contrast, two-site arrays showed low blocking efficiency (9% ± 8%, N = 44), with Rap1 passed into the loop in most cases (Figure 2F). The Rap1 DNA-binding domain (DBD; fragments 310–608) on the 16 Rap1-site array also blocked extrusion effectively (72% ± 11%, N = 65), indicating that dense protein coverage by Rap1 or solely its DBD is sufficient to stall condensin.

By contrast, sparse Rap1 arrays with 35-bp gaps between Rap1 tandems (Figure 1) showed low blocking efficiency (12% ± 9%, N = 49) similar to arrays with only two sites. Inserting LacI protein into the gaps of the sparse array restored high blocking efficiency (88% ± 7%, N = 88), showing that the linear protein filament efficiently blocks DNA loop extrusion. To confirm that high-density blocking is not Rap1 specific, we engineered a dense LacO array, used our sparse Rap1 array as a sparse LacI array, and repeated single-molecule experiments. The sparse LacI array had 8 LacI dimers spaced by 41 bp (477 bp total, 162 nm). The dense LacO array contained 16 sites spaced by 12 bp (548 bp total, 186 nm; Table S2). The sparse LacI arrays blocked condensin at low efficiency (37% ± 12%, N = 67), while the dense array showed high blocking (91% ± 6%, N = 78). In excellent agreement with the *in vivo* findings (Figures 1C and S3), these experiments demonstrate that stalling arises from high local protein density of any type. The experiments with truncated Rap1 (DBD) and LacI show that stalling stems from physical, not biochemical, interactions with condensin.

Stalling of loop extrusion depends on array density, array length, and DNA tension

To investigate the biophysical mechanism of loop extrusion stalling by Rap1 arrays, we tested how stalling depends on array density, array length, and tension. We varied array density by using Rap1 arrays with increasingly larger gaps in between Rap1 pairs (Figure 1B). Given our prior observation that cohesin is blocked by CTCF in a tension-dependent manner,[35] we measured blocking efficiency across a DNA tension range of 0–0.2 pN—well below the stalling threshold of condensin (<0.5 pN).[59]

Blocking efficiency decreased approximately linearly with gap size in all force regimes (Figure 3A). At higher tensions (>0.13 pN), near-complete blocking occurred with the densest array (6-bp gaps), but fell monotonously to ~10% for the 35-bp gap array. Lower DNA tension reduced blocking efficiency across all densities. The monotonous decrease with gap size showed no threshold behavior, suggesting the lack of a discrete enabling gap size.

To dissect the role of array length, we next tested dense arrays (6-bp gaps) with 2, 6, 8, 16, and 32 Rap1 sites (10–188 nm; Table S2). Blocking efficiency increased strongly with array length

Figure 2. Dense Rap1 arrays block loop-extruding condensin in single-molecule experiments

(A) Schematic of a 42-kb linearized DNA molecule with a Rap1 array, tethered to glass through biotin-streptavidin.

(B) Example of a stalling event. Side-flow images of DNA (cyan) and Rap1 array (red). Time points represent initial Rap1 position, loop initiation, loop-Rap1 encounter, and final positions under maximal flow, with array at loop bases for blocking events or inside loops for passing events.

(C) Same as (B), but for a passing event.

(D) Kymograph of a blocking event without applied flow. Normalized DNA and Rap1 positions, loop-Rap1 distance (black), and 51-frame moving MSD of Rap1 (red) are shown. Bottom: loop size (kb), calculated from loop-to-DNA fluorescence intensity ratio.

(E) Same as (D), for a passing event.

(F) Blocking fraction for various Rap1 arrays. DBD, Rap1 DNA-binding domain truncation. +LacI, LacI protein. Error bars: 95% binomial confidence interval. $^{***}p < 10^{-3}$; *ns*, not significant (Fisher exact test).

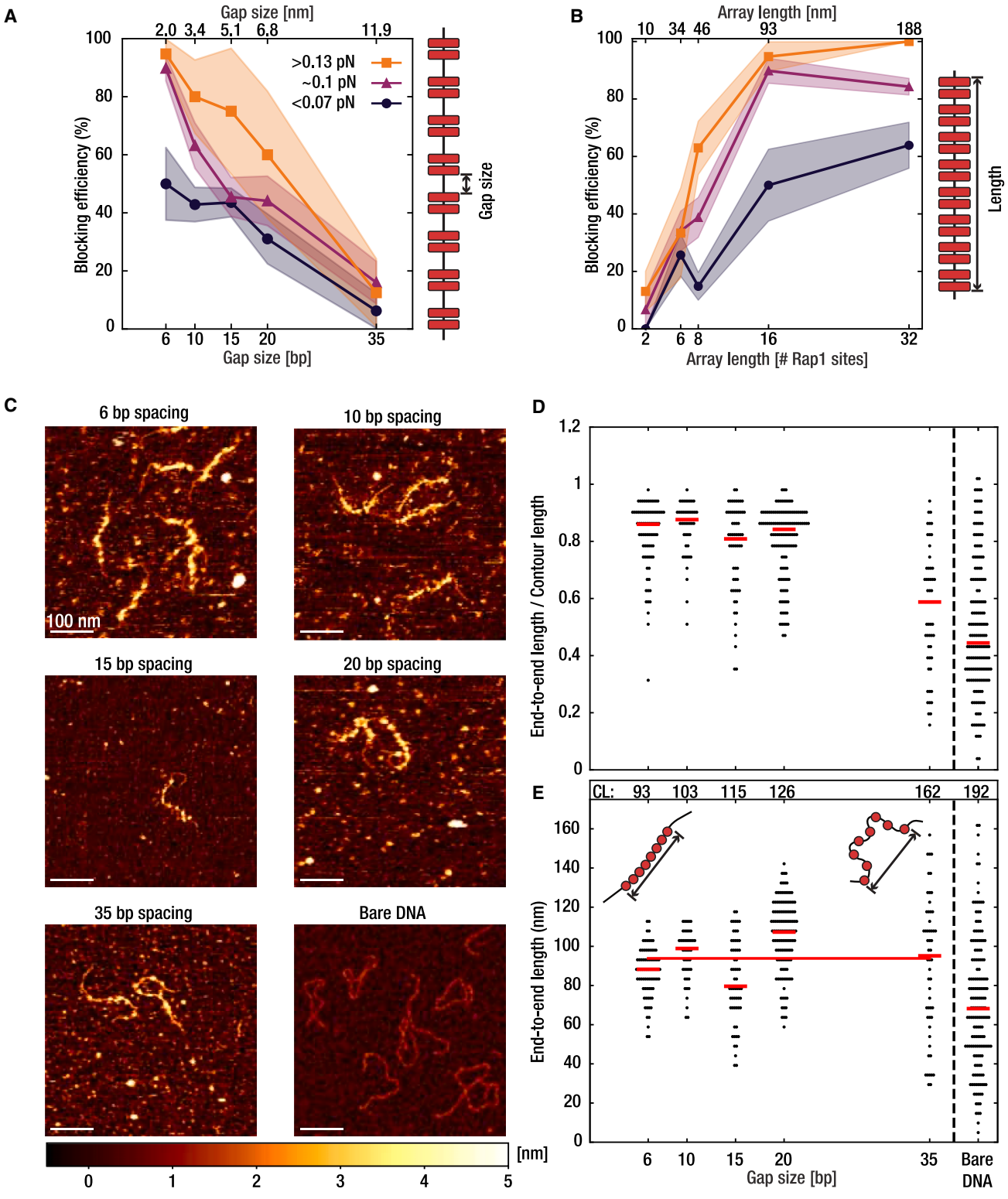

Figure 3. Rap1 array density and length modulate condensin stalling efficiency

(A) Blocking efficiency of 16-site Rap1 arrays across different gap size, shown for three force ranges. Shaded areas represent standard error of proportion.

(B) Blocking efficiency versus array length, for constant 6-bp gap (16-site data same as in A and in Figure 2F).

(legend continued on next page)

for all force regimes (Figure 3B). While blocking was negligible with short arrays, the 16× and 32× Rap1 arrays were highly effective. Interestingly, the impact of tension on blocking was more pronounced for longer arrays, suggesting that local DNA bending, which is hampered under DNA tension, plays a role in loop extrusion.[18,31,32]

These data show that stalling depends on both Rap1 array density and length. Notably, in the lowest force regime, even the longest dense arrays (32× Rap1, 6-bp gaps) can still pass into the loop in ~35% of encounters. This suggests that condensin can occasionally grab DNA beyond the 188-nm array, consistent with previous observations that condensin occasionally steps beyond its ~40-nm diameter.[59,60] Indeed, further analysis of the passing events revealed that some condensin briefly stalled (1–10 s; e.g., Figure S6A) before progressing. While increasing intra-array spacing did not impact transient stalling (Figure S6B), longer arrays led to more condensin complexes exhibiting this behavior (Figure S6C). These findings are consistent with loop extrusion involving large conformational changes in condensin,[18,30,32] as well as the dynamics of the Rap1-bound DNA governed by thermal fluctuations and polymer stiffness. Next, we turned to investigate how Rap1 influences the polymer properties of DNA.

To investigate how Rap1 arrays influence DNA stiffness, we analyzed arrays using atomic force microscopy (AFM). Figure 3C shows typical images for arrays of varying gap sizes. Arrays with 16 Rap1 protein and 6- to 20-bp gaps behaved as fairly stiff rods (in accordance with previous work[61]), whereas flexibility increased at 35-bp spacing, approaching bare DNA (Figures 3C–3E). We quantified stiffness by measuring the end-to-end lengths and normalizing to the contour length (Figure 3D). For the densest arrays, the normalized end-to-end length approached unity, indicating rod-like behavior with minimal bending. Since the end-to-end length is weakly sensitive to stiffness at this scale, exact stiffness values could not be determined. Still, the drop to ~0.6 for 35-bp gap arrays, with broader distribution, points to greater flexibility. Interestingly, the absolute end-to-end length (Figure 3E) remained approximately constant with gap size. As illustrated in the insets, this implies that the 6-bp array—shorter in contour length (93 nm)—is as extended as the more flexible 35-bp array, which has a longer contour (162 nm). Thus, we conclude that denser arrays are also stiffer, which may contribute to their loop extrusion blocking efficiency.

Condensin stalling at dense Rap1 arrays induces local chromatin decompaction in anaphase

Condensin stalling at Rap1 arrays should change local chromatin compaction in cells where condensin is active. We tested this using microscopy by tagging two chromosomal sites 48-kb apart with LacO and TetO arrays, bound by lacI-mCherry and tetR-GFP, respectively[62] (Figure 4A). By measuring the 2D distance between these spots, we inferred local chromatin folding. As expected, the median distance between these spots decreased during anaphase compared to G1, reflecting compaction. This was abolished in condensin-depleted cells (Figure 4A, *smc2-AID* +IAA), indicating that the compaction was condensin dependent.[22,63–66] Importantly, the FP-labeled arrays do not prevent condensin from compacting the intervening region, likely because their relatively low protein density allowed condensin to bypass them (see Figure S3) or because condensin often initiates loop extrusion within that region.

Inserting a dense Rap1 array (16 sites, 6-bp gaps) between the tagged positions had no impact in G1 (Figure 4A), consistent with low condensin activity and showing that DNA stiffening alone did not alter large-scale compaction. However, in anaphase, insertion of the array increased the inter-spot distance to ~400 nm—equivalent to G1—indicating local chromatin decompaction, all other variables held constant. Lowering Rap1 density restored normal compaction (30-bp gap in Figure 4A). The sensitivity to Rap1 density is consistent with condensin stalling being density dependent and causing chromatin decompaction by preventing the formation of larger loops that would otherwise bring the two spots in closer proximity, effectively limiting their contact.

Preferential breakage of dicentric chromosomes near Rap1 arrays is another anticipated outcome of condensin stalling at the arrays (Figure 4B).[12] We used this readout to test arrays with varying Rap1 densities. Rap1 arrays of 16 binding sites with gaps from 6 to 35 bp were inserted in a conditional dicentric chromosome whose one centromere can be reversibly inactivated by galactose-inducible promoters facing the centromere (Figure 4B). To monitor dicentric breakage by abscission, we reactivated the conditional centromere in cells synchronously released from G1 arrest by turning off the promoters. Cells were harvested either before breakage (nocodazole arrest) or after breakage in the next G1 (alpha factor arrest). Chromosome fragments were separated by pulse field gel electrophoresis and detected by Southern blot. Without Rap1 arrays between centromeres, breakage preferentially occurred near the centromeres (Figure S7).[12,50]

We observed a strong dependence of dicentric breakage on gap size. Only high-density arrays focused breakage at the array, while low-density arrays with 30- and 35-bp gaps did not (Figure 4C). Ectopic expression of bacterial LacI restored strong breakage at 35-bp arrays containing *LacO* sites, as reported previously.[12] This effect was attenuated with a LacI* allele of lower *LacO* affinity (Figure 4C).[67] These results further suggest that continuous high-affinity protein binding along the array on DNA is essential to stall condensin *in vivo* as it is *in vitro* (Figure 2F).

DISCUSSION

This work shows that DNA coverage by a telomere protein strongly modulates condensin loop extrusion *in vivo* and *in vitro*.

(C) Representative AFM images for Rap1 arrays of (A) and for bare DNA.
(D) End-to-end lengths normalized by contour length of Rap1 arrays from AFM.
(E) End-to-end lengths; contour length of each construct shown above in nanometers. Red bars show population median; red line shows average end-to-end length across constructs (93.8 nm).

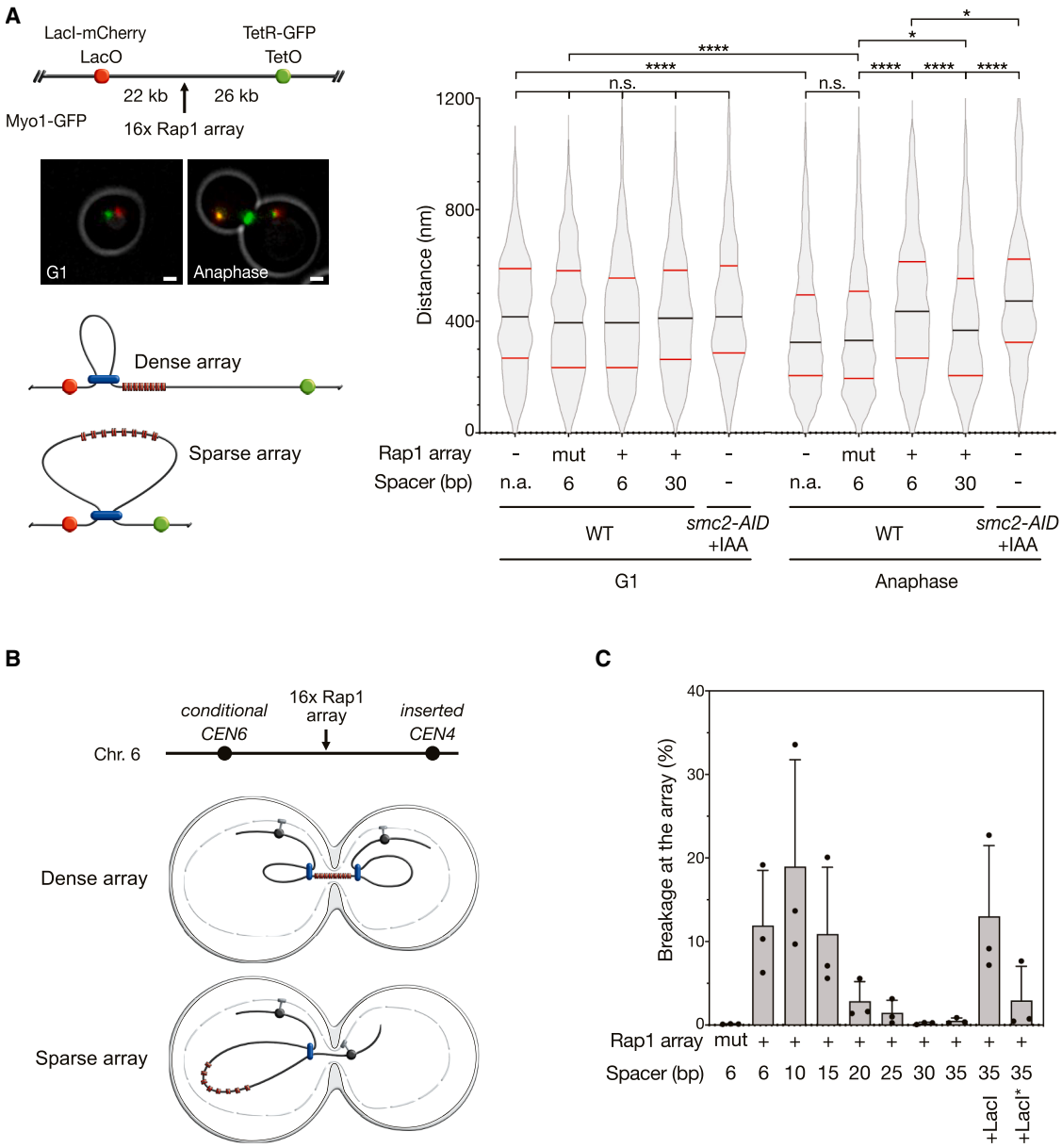

Figure 4. Rap1-bound arrays impact chromatin compaction in anaphase

(A) Telomere-like Rap1 arrays cause local chromatin decompaction in anaphase. Representative images of cells at distinct cell-cycle stages. Anaphase/telophase cells were identified by separated sister chromatids (one in the bud) and an open actomyosin ring (Myo1-GFP) at the bud neck, indicating cytokinesis had not occurred. G1 cells were unbudded. Scale bars: 1 μm (pixel size: 65 nm). Distance between fluorescent spots shown for G1 and anaphase cells. More than 300 cells analyzed per condition. Black lines: median value; red lines: quartiles. Statistical significance via Mann-Whitney test.

(B) Condensin stalling at dense Rap1 arrays in dicentrics focuses entrapment and breakage by abscission.

(C) Dicentric breakage at Rap1-bound arrays with varying gap sizes. Error bars represent standard deviation over three biological replicates. Gels for individual experiments in Figure S7.

Loop-extruding condensin stalls at encounters with telomere-like arrays of Rap1 protein bound on DNA in a length- and density-dependent manner. While individual DNA-bound roadblocks can easily pass into the extruded loop,[38] dense protein coverage halts extrusion. This stalling creates a local boundary to chromosomal compaction during anaphase. Notably, these telomeric protein arrays are remarkably stable as Rap1 residence time on DNA is on the order of hours (Figure S5E), far exceeding the inverse stepping rate of loop extrusion.

Our observations have implications for our biophysical understanding of loop extrusion by SMC complexes. Rap1 binding into a closely spaced array renders the DNA inaccessible to loop

extruders. We found that small gaps facilitate passage, and larger, ~30-bp gaps allow unhindered loop extrusion over the array (Figures 1C, 2F, 3A, and 4). Some condensin complexes briefly pause before bypassing the array, an effect that is more pronounced for longer arrays (Figure S6B).

While the data clearly point to a steric hindrance effect where Rap1 precludes DNA access as a substrate for loop extrusion, Rap1-induced stiffening may also play a role. This stiffening could hinder loop extrusion by increasing the energetic cost of reeling the new DNA within the SMC lumen due to its reduced flexibility—as current models for loop extrusion predict a significant bending of DNA during a loop extrusion step[18,32,59,60,68–71]—and by positioning the next freely accessible DNA further away from condensin, making it harder to reach. While we observed differences between Rap1 arrays of varying length and density, it is difficult to disentangle the effects of density and stiffness; therefore, we cannot determine their relative importance. The data call for a detailed mechanistic model and simulations of loop extrusion with a local array of varying stiffness. Summing up, dense linear protein arrays stall condensin by reducing the amount of accessible DNA that can be grabbed and processed by condensin, as well as potentially by inhibiting the incorporation of the array into the loop and by distancing the accessible DNA to positions beyond the array.

We interpret all the data in the context of a loop extrusion model, which provides a natural explanation of both our *in vivo* and *in vitro* data, as a loop-extruding condensin stalls at dense Rap1 arrays encountered during its linear translocation. An alternative model, diffusion capture,[33,72] proposes that loops form as condensin dynamically encircles one DNA segment to subsequently capture another segment that is genomically distant but physically close by due to polymer dynamics. The array's small size compared to loops that diffusion capture can generate (Figure S8) and the similar end-to-end length of dense and sparse arrays (Figure 3E) suggest that loop extrusion is much more likely than diffusion capture to explain our *in vivo* results. A diffusion capture model would actually predict unhindered loop formation through the grabbing to another region located beyond the array.

Condensin stalling by Rap1 at telomere-telomere fusions favors dicentric breakage near the fusion points. This mechanism provides a backup for telomere protection and contributes to genome stability.[48] As corroborated by microscopy analyses (Figure 4A), a dense Rap1 array causes a local chromatin decompaction in anaphase, consistent with the establishment of a domain boundary resulting from loop extrusion stalling at the array. This reveals a mechanism underlying dicentric breakage at telomere fusions. In anaphase, the connection of centromeres to the spindle poles stretches dicentric anaphase bridges. In telophase, mitotic spindle disassembly and spindle pole detachment from the cell cortex allow condensin to recoil the dicentric bridges.[12,50] Condensin stalling at telomere-telomere fusions will favor the creation of two distinct domains, one in each nuclear lobe. This spatial insulation will direct the telomere-telomere fusion toward the midzone, where the septum grows, thus resulting in its entrapment and breakage by abscission.

Our findings show that the repeated nature of telomeres and the consequential dense DNA coverage yield a unique unidimensional (1D) property: the ability to inhibit protein machines acting along the DNA that could be relevant to other telomere functions. Apart from its role in resolving chromosome fusions, condensin stalling at unfused telomeres may contribute to their accurate segregation (Figure S9). Without stalling, loop extrusion would proceed unhindered until the chromosome ends, where condensin would run off the DNA, leaving the ends uncompacted. Instead, loop extrusion stalling at the chromosome ends, even transiently, would ensure their individualization and proper compaction, facilitating segregation prior to cell division. This function of condensin at telomeres would complement its previously identified role in promoting sister-telomere disjunction.[27,52]

Since extended linear protein filaments stall condensin-driven loop extrusion efficiently, it is of interest to ask whether linear protein filaments more generally block SMCs to extrude loops of DNA. Several observations indicate that this may be the case. DNA repair of double-stranded breaks (DSBs) features a stage where DNA is coated with dense protein arrays, and it has been reported that cohesin accumulates at these filaments.[73,74] While it is commonly assumed that cohesin is specifically loaded at DSB sites,[74] loop extrusion could alternatively play a role in targeting cohesin there.[75,76] Highly transcribed genes slow down loop-extruding SMC complexes,[34,42,43] possibly attributed to a local dense coverage of DNA by RNA polymerases. Finally, the linker length needed for loop extrusion through Rap1 arrays approximates the average spacing between nucleosomes.[77] The tension that condensin can exert on chromatin (<1 pN[15]), insufficient to unwrap nucleosomes,[78] may stretch them,[79,80] which could help to expose internucleosomal DNA for capture by the SMC complex during loop extrusion, a hypothesis that remains to be tested.

Loop extrusion stands as a universally conserved mechanism across the SMC family.[15–17,19,20,32] While we have presented a detailed study of condensin and Rap1 in *S. cerevisiae*, we estimate that our findings have a general significance and likely hold for other SMCs and other protein filaments, providing an important control element for chromosome organization.

Limitations of the study

Our *in vivo* and *in vitro* results show that continuous DNA coverage by proteins is the main determinant stalling condensin. Unavailability of bare DNA within the arrays presents the most obvious explanation. However, DNA local stiffening due to the protein coverage may also contribute to the stalling. A limit of the ChIP assay is that the observed enrichment we attribute to stalling could also stem from a preferential loading of condensin. Nevertheless, our findings by an independent *in vitro* approach that distinguish stalling from loading support the stalling interpretation. Finally, our microscopy-based approach provides static snapshots of chromatin compaction, without capturing dynamic processes. We interpret its results assuming a single loop stalling at the array, which does not consider more complex situations, for instance, two converging loops stalling on each border of the array. More generally, we do not know the density of active condensins in anaphase, how long they remain active, and how long they can remain stalled at array borders before unloading.

RESOURCE AVAILABILITY

Lead contact

Further information and requests for resources should be directed to and will be fulfilled by the lead contact, Stéphane Marcand (stephane.marcand@cea.fr).

Materials availability

Plasmids and yeast strains (Table S1) generated in this study will be available upon request.

Data and code availability

- A selection of the single-molecule imaging data (both whole fields of view and single DNA molecules) has been deposited in the 4TU repository under https://doi.org/10.4121/4dae22e3-0eed-4f9b-8c47-3d4555010e3e.
- No new code was generated for this study.
- Any additional information required to reanalyze the data reported in this paper is available from the lead contact upon request.

ACKNOWLEDGMENTS

We thank Miloš Tišma, Theo Koenig, Eric Le Cam, Olivier Pietrement, Gerard Mazón, Armelle Lengronne, Jonathan Heuze, Olivier Alibert, Stéphane Coulon, Sylvie Tournier, Pascal Bernard, Frédéric Beckouet, Sabrina Pobiega, and Florian Roisné-Hamelin for discussions; Anders Barth for help with determining the Rap1 labeling efficiency; Minco Polinder for help in labeling the DNA covalently; and Eli van der Sluis and Ashmiani van den Berg for purifying condensin and LacI proteins. Research in the laboratory of S.M. was supported by grants from Agence Nationale de la Recherche (ANR-14-CE10-021 DICENS, ANR-15CE12-0007 DNA-Life, and ANR-22-CE12-0037 TELOSTAB), Fondation ARC pour la Recherche sur le Cancer, Ligue contre le Cancer, the CEA radiation biology program, and the GGP CEA Électricité de France (EDF) program. A.D. was supported by CEA and Ligue Nationale contre le Cancer. Research in the laboratory of C.D. was supported by European Research Council Advanced Grant 883684 (DNA looping) NWO grant OCENW.GROOT.2019.012, and the BaSyC program.

AUTHOR CONTRIBUTIONS

B.T.A. co-designed the project, performed single-molecule visualization, data analysis, and manuscript writing. A.D. co-designed the project and performed the Rap1 site array cloning, *in vivo* microscopy, dicentric breakage, data analysis, and manuscript writing. J.v.d.T. cloned constructs for single-molecule visualization and AFM. T.M.G. explored Micro-C and edited the manuscript. A.J.K. performed AFM and data analysis. C. Béneut conducted ChIP and dicentric breakage. R.B. did the initial single-molecule visualization. J.P. and K.D. designed tools used for *in vivo* microscopy and data analysis. V.S. performed the data analysis and edited the manuscript. X.V. and D.B. created the Rap1 expression vector and purified Rap1. S. Mattarocci co-designed the project, did the data analysis, wrote the manuscript, and supervised the project. C.D. co-designed the project, wrote the manuscript and supervised the project. S. Marcand co-designed the project, analyzed data, wrote the manuscript, and supervised the project.

DECLARATION OF INTERESTS

The authors declare no competing interests.

STAR★METHODS

Detailed methods are provided in the online version of this paper and include the following:

SUPPLEMENTAL INFORMATION

Supplemental information can be found online at https://doi.org/10.1016/j.celrep.2025.115900.

Received: November 9, 2024
Revised: April 19, 2025
Accepted: June 3, 2025

REFERENCES

1. de Lange, T. (2018). Shelterin-Mediated Telomere Protection. Annu. Rev. Genet. *52*, 223–247.
2. Wellinger, R.J., and Zakian, V.A. (2012). Everything You Ever Wanted to Know About *Saccharomyces cerevisiae* Telomeres: Beginning to End. Genetics *191*, 1073–1105.
3. Galati, A., Micheli, E., and Cacchione, S. (2013). Chromatin Structure in Telomere Dynamics. Front. Oncol. *3*, 46.
4. Soman, A., Korolev, N., and Nordenskiöld, L. (2022). Telomeric chromatin structure. Curr. Opin. Struct. Biol. *77*, 102492.
5. Negrini, S., Ribaud, V., Bianchi, A., and Shore, D. (2007). DNA breaks are masked by multiple Rap1 binding in yeast: implications for telomere capping and telomerase regulation. Genes Dev. *21*, 292–302.
6. Makovets, S., Herskowitz, I., and Blackburn, E.H. (2004). Anatomy and Dynamics of DNA Replication Fork Movement in Yeast Telomeric Regions. Mol. Cell Biol. *24*, 4019–4031.
7. Miller, K.M., Rog, O., and Cooper, J.P. (2006). Semi-conservative DNA replication through telomeres requires Taz1. Nature *440*, 824–828.
8. Maestroni, L., Reyes, C., Vaurs, M., Gachet, Y., Tournier, S., Géli, V., and Coulon, S. (2020). Nuclear envelope attachment of telomeres limits TERRA and telomeric rearrangements in quiescent fission yeast cells. Nucleic Acids Res. *48*, 3029–3041.
9. Marcand, S., Pardo, B., Gratias, A., Cahun, S., and Callebaut, I. (2008). Multiple pathways inhibit NHEJ at telomeres. Genes Dev. *22*, 1153–1158.
10. Zimmermann, M., Kibe, T., Kabir, S., and de Lange, T. (2014). TRF1 negotiates TTAGGG repeat-associated replication problems by recruiting the BLM helicase and the TPP1/POT1 repressor of ATR signaling. Genes Dev. *28*, 2477–2491.
11. Goto, G.H., Zencir, S., Hirano, Y., Ogi, H., Ivessa, A., and Sugimoto, K. (2015). Binding of Multiple Rap1 Proteins Stimulates Chromosome Breakage Induction during DNA Replication. PLoS Genet. *11*, e1005283.
12. Guérin, T.M., Béneut, C., Barinova, N., López, V., Lazar-Stefanita, L., Deshayes, A., Thierry, A., Koszul, R., Dubrana, K., and Marcand, S. (2019). Condensin-Mediated Chromosome Folding and Internal Telomeres Drive Dicentric Severing by Cytokinesis. Mol. Cell *75*, 131–144.e3.
13. Yatskevich, S., Rhodes, J., and Nasmyth, K. (2019). Organization of Chromosomal DNA by SMC Complexes. Annu. Rev. Genet. *53*, 445–482.
14. Goloborodko, A., Marko, J.F., and Mirny, L.A. (2016). Chromosome Compaction by Active Loop Extrusion. Biophys. J. *110*, 2162–2168.

15. Ganji, M., Shaltiel, I.A., Bisht, S., Kim, E., Kalichava, A., Haering, C.H., and Dekker, C. (2018). Real-time imaging of DNA loop extrusion by condensin. Science *360*, 102–105.

16. Davidson, I.F., Bauer, B., Goetz, D., Tang, W., Wutz, G., and Peters, J.M. (2019). DNA loop extrusion by human cohesin. Science *366*, 1338–1345.

17. Taschner, M., and Gruber, S. (2023). DNA Segment Capture by Smc5/6 Holo-Complexes. Nat. Struct. and Mol. Biol. *30*, 619–628.

18. Shaltiel, I.A., Datta, S., Lecomte, L., Hassler, M., Kschonsak, M., Bravo, S., Stober, C., Ormanns, J., Eustermann, S., and Haering, C.H. (2022). A hold-and-feed mechanism drives directional DNA loop extrusion by condensin. Science *376*, 1087–1094.

19. Liu, H.W., Roisné-Hamelin, F., Beckert, B., Li, Y., Myasnikov, A., and Gruber, S. (2022). DNA-measuring Wadjet SMC ATPases restrict smaller circular plasmids by DNA cleavage. Mol. Cell *82*, 4727–4740.e6.

20. Pradhan, B., Kanno, T., Igarashi, M.U., Baaske, M.D., Kei Wong, J.S., Jeppsson, K., Björkegren, C., and Kim, E. (2023). The Smc5/6 Complex Is a DNA Loop Extruding Motor. Nature *616*, 843–848.

21. Lioy, V.S., Cournac, A., Marbouty, M., Duigou, S., Mozziconacci, J., Espéli, O., Boccard, F., and Koszul, R. (2018). Multiscale Structuring of the E. coli Chromosome by Nucleoid-Associated and Condensin Proteins. Cell *172*, 771–783.e18.

22. Lazar-Stefanita, L., Scolari, V.F., Mercy, G., Muller, H., Guérin, T.M., Thierry, A., Mozziconacci, J., and Koszul, R. (2017). Cohesins and condensins orchestrate the 4D dynamics of yeast chromosomes during the cell cycle. EMBO J. *36*, 2684–2697.

23. Shintomi, K., Inoue, F., Watanabe, H., Ohsumi, K., Ohsugi, M., and Hirano, T. (2017). Mitotic chromosome assembly despite nucleosome depletion in *Xenopus* egg extracts. Science *356*, 1284–1287.

24. Gibcus, J.H., Samejima, K., Goloborodko, A., Samejima, I., Naumova, N., Nuebler, J., Kanemaki, M.T., Xie, L., Paulson, J.R., Earnshaw, W. C., et al. (2018). A pathway for mitotic chromosome formation. Science *359*, eaao6135.

25. Dey, A., Shi, G., Takaki, R., and Thirumalai, D. (2023). Structural changes in chromosomes driven by multiple condensin motors during mitosis. Cell Rep. *42*, 112348.

26. Cuylen, S., Metz, J., Hruby, A., and Haering, C.H. (2013). Entrapment of Chromosomes by Condensin Rings Prevents Their Breakage during Cytokinesis. Dev. Cell *27*, 469–478.

27. Renshaw, M.J., Ward, J.J., Kanemaki, M., Natsume, K., Nédélec, F.J., and Tanaka, T.U. (2010). Condensins Promote Chromosome Recoiling during Early Anaphase to Complete Sister Chromatid Separation. Dev. Cell *19*, 232–244.

28. Lee, B.-G., Rhodes, J., and Löwe, J. (2022). Clamping of DNA shuts the condensin neck gate. Proc. Natl. Acad. Sci. USA *119*, e2120006119.

29. Kschonsak, M., Merkel, F., Bisht, S., Metz, J., Rybin, V., Hassler, M., and Haering, C.H. (2017). Structural Basis for a Safety-Belt Mechanism That Anchors Condensin to Chromosomes. Cell *171*, 588–600.e24.

30. Diebold-Durand, M.-L., Lee, H., Ruiz Avila, L.B., Noh, H., Shin, H.C., Im, H., Bock, F.P., Bürmann, F., Durand, A., Basfeld, A., et al. (2017). Structure of Full-Length SMC and Rearrangements Required for Chromosome Organization. Mol. Cell *67*, 334–347.e5.

31. Nomidis, S.K., Carlon, E., Gruber, S., and Marko, J.F. (2022). DNA tension-modulated translocation and loop extrusion by SMC complexes revealed by molecular dynamics simulations. Nucleic Acids Res. *50*, 4974–4987.

32. Dekker, C., Haering, C.H., Peters, J.-M., and Rowland, B.D. (2023). How do molecular motors fold the genome? Science *382*, 646–648.

33. Higashi, T.L., and Uhlmann, F. (2022). SMC complexes: Lifting the lid on loop extrusion. Curr. Opin. Cell Biol. *74*, 13–22.

34. Brandão, H.B., Paul, P., van den Berg, A.A., Rudner, D.Z., Wang, X., and Mirny, L.A. (2019). RNA polymerases as moving barriers to condensin loop extrusion. Proc. Natl. Acad. Sci. USA *116*, 20489–20499.

35. Davidson, I.F., Barth, R., Zaczek, M., van der Torre, J., Tang, W., Nagasaka, K., Janissen, R., Kerssemakers, J., Wutz, G., Dekker, C., and Peters, J.M. (2023). CTCF is a DNA-tension-dependent barrier to cohesin-mediated loop extrusion. Nature *616*, 822–827.

36. Wendt, K.S., Yoshida, K., Itoh, T., Bando, M., Koch, B., Schirghuber, E., Tsutsumi, S., Nagae, G., Ishihara, K., Mishiro, T., et al. (2008). Cohesin mediates transcriptional insulation by CCCTC-binding factor. Nature *451*, 796–801.

37. Li, Y., Haarhuis, J.H.I., Sedeño Cacciatore, Á., Oldenkamp, R., van Ruiten, M.S., Willems, L., Teunissen, H., Muir, K.W., de Wit, E., Rowland, B.D., and Panne, D. (2020). The structural basis for cohesin–CTCF-anchored loops. Nature *578*, 472–476.

38. Pradhan, B., Barth, R., Kim, E., Davidson, I.F., Bauer, B., van Laar, T., Yang, W., Ryu, J.K., van der Torre, J., Peters, J.M., and Dekker, C. (2022). SMC complexes can traverse physical roadblocks bigger than their ring size. Cell Rep. *41*, 111491.

39. Nanni, L., Ceri, S., and Logie, C. (2020). Spatial patterns of CTCF sites define the anatomy of TADs and their boundaries. Genome Biol. *21*, 197.

40. Liu, H.W., Roisné-Hamelin, F., Taschner, M., Collier, J., Srinivasan, M., and Gruber, S. (2025). The SMC Hinge is a Selective Gate for Obstacle Bypass. Preprint at bioRxiv. https://doi.org/10.1101/2025.03.17.643644.

41. Rivosecchi, J., Jost, D., Vachez, L., Gautier, F.D., Bernard, P., and Vanoosthuyse, V. (2021). RNA polymerase backtracking results in the accumulation of fission yeast condensin at active genes. Life Sci. Alliance *4*, e202101046.

42. Banigan, E.J., Tang, W., van den Berg, A.A., Stocsits, R.R., Wutz, G., Brandão, H.B., Busslinger, G.A., Peters, J.M., and Mirny, L.A. (2023). Transcription shapes 3D chromatin organization by interacting with loop extrusion. Proc. Natl. Acad. Sci. USA *120*, e2210480120.

43. Lebreton, J., Colin, L., Chatre, E., and Bernard, P. (2024). RNA Pol II antagonises mitotic chromatin folding and chromosome segregation by condensin. Cell Rep. *43*, 113901.

44. Zhang, H., Shi, Z., Banigan, E.J., Kim, Y., Yu, H., Bai, X.C., and Finkelstein, I.J. (2023). CTCF and R-loops are boundaries of cohesin-mediated DNA looping. Mol. Cell *83*, 2856–2871.e8.

45. Lengronne, A., Katou, Y., Mori, S., Yokobayashi, S., Kelly, G.P., Itoh, T., Watanabe, Y., Shirahige, K., and Uhlmann, F. (2004). Cohesin relocation from sites of chromosomal loading to places of convergent transcription. Nature *430*, 573–578.

46. Bausch, C., Noone, S., Henry, J.M., Gaudenz, K., Sanderson, B., Seidel, C., and Gerton, J.L. (2007). Transcription Alters Chromosomal Locations of Cohesin in Saccharomyces cerevisiae. Mol. Cell Biol. *27*, 8522–8532.

47. Paldi, F., Alver, B., Robertson, D., Schalbetter, S.A., Kerr, A., Kelly, D.A., Baxter, J., Neale, M.J., and Marston, A.L. (2020). Convergent genes shape budding yeast pericentromeres. Nature *582*, 119–123.

48. Pobiega, S., and Marcand, S. (2010). Dicentric breakage at telomere fusions. Genes Dev. *24*, 720–733.

49. Guérin, T.M., and Marcand, S. (2022). Breakage in breakage–fusion–bridge cycle: an 80-year-old mystery. Trends Genet. *38*, 641–645.

50. Lopez, V., Barinova, N., Onishi, M., Pobiega, S., Pringle, J.R., Dubrana, K., and Marcand, S. (2015). Cytokinesis breaks dicentric chromosomes preferentially at pericentromeric regions and telomere fusions. Genes Dev. *29*, 322–336.

51. Grossi, S., Bianchi, A., Damay, P., and Shore, D. (2001). Telomere Formation by Rap1p Binding Site Arrays Reveals End-Specific Length Regulation Requirements and Active Telomeric Recombination. Mol. Cell Biol. *21*, 8117–8128.

52. Colin, L., Reyes, C., Berthezene, J., Maestroni, L., Modolo, L., Toselli, E., Chanard, N., Schaak, S., Cuvier, O., Gachet, Y., et al. (2023). Condensin positioning at telomeres by shelterin proteins drives sister-telomere disjunction in anaphase. eLife *12*, RP89812.

53. Leonard, J., Sen, N., Torres, R., Sutani, T., Jarmuz, A., Shirahige, K., and Aragón, L. (2015). Condensin Relocalization from Centromeres to

Chromosome Arms Promotes Top2 Recruitment during Anaphase. Cell Rep. *13*, 2336–2344.

54. Kim, J.H., Zhang, T., Wong, N.C., Davidson, N., Maksimovic, J., Oshlack, A., Earnshaw, W.C., Kalitsis, P., and Hudson, D.F. (2013). Condensin I associates with structural and gene regulatory regions in vertebrate chromosomes. Nat. Commun. *4*, 2537.
55. Williams, T.L., Levy, D.L., Maki-Yonekura, S., Yonekura, K., and Blackburn, E.H. (2010). Characterization of the Yeast Telomere Nucleoprotein Core. J. Biol. Chem. *285*, 35814–35824.
56. Falcon, C.M., and Matthews, K.S. (1999). Glycine Insertion in the Hinge Region of Lactose Repressor Protein Alters DNA Binding. J. Biol. Chem. *274*, 30849–30857.
57. Matot, B., Le Bihan, Y.V., Lescasse, R., Pérez, J., Miron, S., David, G., Castaing, B., Weber, P., Raynal, B., Zinn-Justin, S., et al. (2012). The orientation of the C-terminal domain of the Saccharomyces cerevisiae Rap1 protein is determined by its binding to DNA. Nucleic Acids Res. *40*, 3197–3207.
58. Lickwar, C.R., Mueller, F., Hanlon, S.E., McNally, J.G., and Lieb, J.D. (2012). Genome-wide protein–DNA binding dynamics suggest a molecular clutch for transcription factor function. Nature *484*, 251–255.
59. Ryu, J.-K., Rah, S.H., Janissen, R., Kerssemakers, J.W.J., Bonato, A., Michieletto, D., and Dekker, C. (2022). Condensin extrudes DNA loops in steps up to hundreds of base pairs that are generated by ATP binding events. Nucleic Acids Res. *50*, 820–832.
60. Takaki, R., Dey, A., Shi, G., and Thirumalai, D. (2021). Theory and simulations of condensin mediated loop extrusion in DNA. Nat. Commun. *12*, 5865.
61. Le Bihan, Y.-V., Matot, B., Pietrement, O., Giraud-Panis, M.J., Gasparini, S., Le Cam, E., Gilson, E., Sclavi, B., Miron, S., and Le Du, M.H. (2013). Effect of Rap1 binding on DNA distortion and potassium permanganate hypersensitivity. Acta Crystallogr. D Biol. Crystallogr. *69*, 409–419.
62. Phipps, J., Toulouze, M., Ducrot, C., Costa, R., Brocas, C., and Dubrana, K. (2025). Cohesin complex oligomerization maintains end-tethering at DNA double-strand breaks. Nat. Cell Biol. *27*, 118–129.
63. Lamothe, R., Costantino, L., and Koshland, D.E. (2020). The spatial regulation of condensin activity in chromosome condensation. Genes Dev. *34*, 819–831.
64. Bystricky, K., Heun, P., Gehlen, L., Langowski, J., and Gasser, S.M. (2004). Long-range compaction and flexibility of interphase chromatin in budding yeast analyzed by high-resolution imaging techniques. Proc. Natl. Acad. Sci. USA *101*, 16495–16500.
65. Vas, A.C.J., Andrews, C.A., Kirkland Matesky, K., and Clarke, D.J. (2007). In Vivo Analysis of Chromosome Condensation in *Saccharomyces cerevisiae*. MBoC *18*, 557–568.
66. Robellet, X., Thattikota, Y., Wang, F., Wee, T.L., Pascariu, M., Shankar, S., Bonneil, É., Brown, C.M., and D'Amours, D. (2015). A high-sensitivity phospho-switch triggered by Cdk1 governs chromosome morphogenesis during cell division. Genes Dev. *29*, 426–439.
67. Dubarry, M., Loïodice, I., Chen, C.L., Thermes, C., and Taddei, A. (2011). Tight protein–DNA interactions favor gene silencing. Genes Dev. *25*, 1365–1370.
68. Oldenkamp, R., and Rowland, B.D. (2022). A walk through the SMC cycle: From catching DNAs to shaping the genome. Mol. Cell *82*, 1616–1630. https://doi.org/10.1016/J.MOLCEL.2022.04.006.
69. Kim, E., Barth, R., and Dekker, C. (2023). Looping the Genome with SMC Complexes. Annu. Rev. Biochem. *92*, 15–41.
70. Higashi, T.L., Pobegalov, G., Tang, M., Molodtsov, M.I., and Uhlmann, F. (2021). A Brownian ratchet model for DNA loop extrusion by the cohesin complex. eLife *10*, e67530.
71. Bauer, B.W., Davidson, I.F., Canena, D., Wutz, G., Tang, W., Litos, G., Horn, S., Hinterdorfer, P., and Peters, J.M. (2021). Cohesin mediates DNA loop extrusion by a "swing and clamp" mechanism. Cell *184*, 5448–5464.e22.
72. Tang, M., Pobegalov, G., Tanizawa, H., Chen, Z.A., Rappsilber, J., Molodtsov, M., Noma, K.I., and Uhlmann, F. (2023). Establishment of dsDNA-dsDNA interactions by the condensin complex. Mol. Cell *83*, 3787–3800.e9.
73. Ström, L., Lindroos, H.B., Shirahige, K., and Sjögren, C. (2004). Postreplicative Recruitment of Cohesin to Double-Strand Breaks Is Required for DNA Repair. Mol. Cell *16*, 1003–1015.
74. Phipps, J., and Dubrana, K. (2022). DNA Repair in Space and Time: Safeguarding the Genome with the Cohesin Complex. Genes *13*, 198.
75. Haarhuis, J.H.I., van der Weide, R.H., Blomen, V.A., Yáñez-Cuna, J.O., Amendola, M., van Ruiten, M.S., Krijger, P.H.L., Teunissen, H., Medema, R.H., van Steensel, B., et al. (2017). The Cohesin Release Factor WAPL Restricts Chromatin Loop Extension. Cell *169*, 693–707.e14.
76. Haarhuis, J.H., and Rowland, B.D. (2017). Cohesin: building loops, but not compartments. EMBO J. *36*, 3549–3551.
77. Brogaard, K., Xi, L., Wang, J.-P., and Widom, J. (2012). A map of nucleosome positions in yeast at base-pair resolution. Nature *486*, 496–501.
78. Ngo, T.T.M., Zhang, Q., Zhou, R., Yodh, J.G., and Ha, T. (2015). Asymmetric Unwrapping of Nucleosomes under Tension Directed by DNA Local Flexibility. Cell *160*, 1135–1144.
79. Marko, J.F., and Siggia, E.D. (1994). Bending and twisting elasticity of DNA. Macromolecules *27*, 981–988.
80. Kaczmarczyk, A., Allahverdi, A., Brouwer, T.B., Nordenskiöld, L., Dekker, N.H., and van Noort, J. (2017). Single-molecule force spectroscopy on histone H4 tail-cross-linked chromatin reveals fiber folding. J. Biol. Chem. *292*, 17506–17513.
81. Roisné-Hamelin, F., Pobiega, S., Jézéquel, K., Miron, S., Dépagne, J., Veaute, X., Busso, D., Du, M.H.L., Callebaut, I., Charbonnier, J.B., et al. (2021). Mechanism of MRX inhibition by Rif2 at telomeres. Nat. Commun. *12*, 2763.
82. Lescasse, R., Pobiega, S., Callebaut, I., and Marcand, S. (2013). End-joining inhibition at telomeres requires the translocase and polySUMO-dependent ubiquitin ligase Uls1. EMBO J. *32*, 805–815.
83. Tišma, M., Panoukidou, M., Antar, H., Soh, Y.M., Barth, R., Pradhan, B., Barth, A., van der Torre, J., Michieletto, D., Gruber, S., and Dekker, C. (2022). ParB proteins can bypass DNA-bound roadblocks via dimer-dimer recruitment. Sci. Adv. *8*, eabn3299.
84. St-Pierre, J., Douziech, M., Bazile, F., Pascariu, M., Bonneil, E., Sauvé, V., Ratsima, H., and D'Amours, D. (2009). Polo Kinase Regulates Mitotic Chromosome Condensation by Hyperactivation of Condensin DNA Supercoiling Activity. Mol. Cell *34*, 416–426.
85. The condensin complex is a mechanochemical motor that translocates along DNA | Science. https://www.science.org/doi/10.1126/science.aan6516?url_ver=Z39.88-2003&rfr_id=ori:rid:crossref.org&rfr_dat=cr_pub%20%200pubmed.
86. Liu, H. & Shima, T. 2021. A Fast and Objective Hidden Markov Modeling for Accurate Analysis of Biophysical Data with Numerous States. https://doi.org/10.1101/2021.05.30.446337.
87. Nečas, D., and Klapetek, P. (2012). Gwyddion: an open-source software for SPM data analysis. Open Phys. *10*, 181–188.
88. Pradhan, B., Barth, R., and Analikwu, B.T. (2023). biswajitSM/LEADS: Encounter of SMCs with a Roadblock. Zenodo. https://doi.org/10.5281/zenodo.7634719.
89. Bouchiat, C., Wang, M.D., Allemand, J., Strick, T., Block, S.M., and Croquette, V. (1999). Estimating the Persistence Length of a Worm-Like Chain Molecule from Force-Extension Measurements. Biophys. J. *76*, 409–413.

STAR★METHODS

KEY RESOURCES TABLE

REAGENT or RESOURCE	SOURCE	IDENTIFIER
Experimental models: Organisms/strains		
Saccharomyces cerevisiae	This study	Listed in Table S1
Chemicals and recombinant proteins		
APTMS ((3-Aminopropyl)trimethoxysilane)	Sigma	281778
Methyl-PEG4-NHS Esther	Fisher Scientific	22341
Biotin-PEG-SVA, MW 5000	Laysan Bio	Biotin-PEG-SVA-5000
MPEG-SVA-5000	Laysan Bio	MPEG-SVA-5000
Streptavidin	Fisher Scientific	10700995
Trolox ((±)-6-Hydroxy-2,5,7, 8-tetramethylchromane-2-carboxylic acid)	Sigma	238813
Glucose oxidase	MP Biomedicals	195196
Catalase from bovine liver	Sigma	C30
ATP	Thermo Scientific	R0441
BSA	Thermo Scientific	AM2618
Sytox orange	Thermo Scientific	S11368
Janelia Fluor 646, maleimide	Bio-Techne	6590
Poly-L-Lysine 0.01%	Sigma	P4707
Mica sheet V4	Electron Microscopy Sciences	71853-05
PeakForce-Hirs-F-B cantilevers	Bruker	3958
Yeast nitrogen base	Difco BD	291940
Casamino acids	Difco BD	228830
Leucine	Sigma	L8000
Tyrosine	Sigma	T3754
D-glucose	Sigma	G8270
Raffinose	Biosynth	R-1000
D-galactose	Biosynth	G-1700
alpha-factor	Sigma-Aldrich	T6901
Nocodazole	Sigma-Aldrich	M1404
GelRed	Biotium	41003-1
Zymolyase-100T	MP Biomedical	32093
Proteinase K	Invitrogen	P/N 100005393
dCTP-alpha-32P 6000 Ci/mmol	PerkinElmer	BLU-513Z
Indole-3-acetic acid (IAA) sodium salt (Auxin)	Sigma-Aldrich	I2886
Talon Superflow resin	Cytiva	28-9575-02
Imidazole	Sigma	I202
MWCO 10 kDa Vivaspin 20	Sigma	Z614610
Superdex 200 Increase 10/300 column	Cytiva	28990944
Sephacryl S-1000 SF, Tricorn 10/600 GL	Cytiva	28925627
His6-TEV-4G-ScRap1-1-827	This work	N/A
His6-TEV-4G-ScRap1-310-608	This work	N/A
Condensin	Ganji et al.[15]	N/A
LacI-SNAP	This work	N/A
Deposited data		
Selection of the single-molecule imaging data	This study	4TU repository https://doi.org/10.4121/4dae22e3-0eed-4f9b-8c47-3d4555010e3e

(*Continued on next page*)

Continued

REAGENT or RESOURCE	SOURCE	IDENTIFIER
Recombinant DNA		
Rap1/LacI binding site arrays	This study	Listed in Table S2
Software and algorithms		
Fiji	NIH	Version 2.9.0
Python	https://www.python.org	Version 3.9
Gwyddion	http://www.gwyddion.net	Version 2.66
Prism	GraphPad	Version 10
Distiller	https://github.com/open2c/distiller-nf	Commit 8aa86e
LEADS	https://github.com/biswajitSM/LEADS	v1.0.0
Image J	Wayne Rasband	https://imagej.nih.gov/ij/
Metamorph	Molecular Devices	https://www.moleculardevices.com

EXPERIMENTAL MODEL

S. cerevisiae strains used for all the *in vivo* experiments are of the W303 genetic background and their genotypes are listed in Table S1. Strains were transformed by the lithium acetate method. Rap1 arrays were inserted in intergenic regions and their insertion did not impact cell growth nor cell cycle progression. All transformants were sequenced for correct introduction of the insert and preservation of the remaining of the targeted region.

METHOD DETAILS

Cell cycle synchronization

To synchronized cells in late anaphase (ChIP experiments), exponentially growing cells carrying the *cdc15-2* thermosensitive allele were arrested at restrictive temperature (36°C) for about 90 minutes prior to be shifted back at permissive temperature (25°C) for 30 minutes. Cell cycle arrest in anaphase at restrictive temperature was monitored using microscopy, ensuring that fewer than 1% cells displayed no bud or a small bud. We also verified the quality of the release at the permissive temperature, with bud emergence occurring 60-70 minutes after the temperature shift. Cytokinesis takes place between 40 and 60 minutes after the shift to the permissive temperature.

To assess dicentric breakage, cells growing exponentially in galactose-containing synthetic medium (*CEN6* OFF) were arrested in G1 with α-factor (10^{-7} M). Cells were released from the G1 arrest with two washes in glucose-containing rich medium (YPD). Half the culture was complemented with nocodazole (5 μg/mL) to arrest the cells in G2/M. The other half was complemented with α-factor (10^{-7} M) about one hour after the washes to arrest the cells in the next G1.

Pulse-field gel electrophoresis

Yeast DNA embedded in agarose plugs was prepared as described[12] with minor modification (see supplemental information). Pulse-field gel electrophoresis was carried out in a 0.9% agarose gel in 0.5× TBE at 14°C with a CHEF DR III from Bio-Rad with a constant switch time of 20 s during 24 h. Gel-Red labeled DNA was detected by a Typhoon scanner. DNA transferred to a nitrocellulose member was hybridized with ^{32}P-labeled *TUB2* (chr. 6 probe) and *POL4* (chr. 3 probe) fragment as previously described.[12]

Distance measurements by microscopy of cells

Exponential growing cells (0.8 OD) in rich medium (YPD) were washed in synthetic medium prior to live-cell imaging with a wide-field inverted microscope (Leica DMI-6000B) equipped with Adaptive Focus Control to eliminate Z drift, a 100×/1.4 NA immersion objective with a Prior NanoScanZ Nanopositioning Piezo Z Stage System, a CMOS camera (ORCA-Flash4.0; Hamamatsu), and a solid-state light source (SpectraX, Lumencore). The system is piloted by MetaMorph software (Molecular Device). 2mM Indole-3-acetic acid (IAA) was added to exponential growing *smc2-AID* cells in YPD for 1 hour prior to imaging.

GFP and mCherry two-color images were acquired over 19 focal steps of 0.2μm using solid state 475 and 575nm diodes and appropriate filters (GFP-mRFP filter; excitation: double BP, 450–490/550–590nm and dichroic double BP 500–550/600–665nm; Chroma Technology Corp.). Acquisition of both wavelengths was completed on each focal plane with an exposure time of 50ms, before 0.2μm steps, to minimise the possibility of array movement between acquisitions of each wavelength. A single bright-field image on one focal plane was acquired at each time point with an exposure of 50ms. All images shown are maximum intensity z projections of z-stack images.

Image analysis was achieved following processing with ImageJ Fiji software, using scripts written in ImageJ macro language. Briefly, local maxima that define GFP and mCherry fluorescent array positions were determined from 2D maximal projections of three-dimensional data sets. Fluorescent signals within cells were confirmed manually from 3 color merged images. The distance between the two closest GFP and mCherry maxima was calculated using their extracted XY coordinates in R software (v4.1.1).

ChIP

ChIP experiments were carried out as previously described with minor modifications.[81,82]

DNA preparation for single-molecule assay

42-kb Linear cosmid-i95 plasmids with inserted sequences were prepared as previously reported.[38,83] First, the i95-cosmid was linearized with PsiI-v2 (New England Biolabs). Second, the remaining 5'-phosphate groups were dephosphorylated using calf-intestinal alkaline phosphatase for 10 minutes at 37°C and finally heat inactivated for 20 min at 80°C (Quick CIP, New England Biolabs). The Rap1 arrays initially cloned in a pUC19-derived vector (Table S2) were digested with PvuII (New England Biolabs) and subsequently gel isolated. The fragments were ligated together by using a T4 DNA ligase in T4 ligase buffer (New England Biolabs), with 1 mM ATP overnight at 16°C. The final constructs were transformed into *E. coli* NEB 10-beta cells (New England Biolabs) and all constructs were sequence verified using plasmidsaurus Oxford Nanopore long read sequencing. Inserted sequences are listed in Table S2. To linearize these cosmids and prepare them for flow cell insertion, the cosmids were isolated using a Midiprep and a QIAfilter plasmid midi kit (QIAGEN). The cosmids were then digested for 2 hours at 37°C and heat-inactivated for 20 minutes at 80°C using SpeI-HF (New England Biolabs). Next, 5'-biotin handles were constructed by a PCR reaction from a pBluescript SK+ (StrataGene) using 5'-biotin primers JT337 (Bio- AGAATAGACCGAGATAGGGTTGAGTG) and JT338 (Bio-GGCAGGGTCGGAACAGGAGAG). The PCR fragment was then digested by the same procedure as for the large cosmid, resulting in ~600-bp 5'-biotin handles, which were mixed with the digested cosmids in a 10x excess before ligation by T4 DNA ligase in T4 ligase buffer (New England Biolabs) at 16°C overnight. The reaction was subsequently heat-inactivated at 65°C for 25 min. The final linear construct was cleaned-up using an ÄKTA Start (Cytiva), with a homemade gel filtration column containing 46 mL of Sephacryl S-1000 SF gel filtration media, run with TE + 150 mM NaCl buffer at 0.5 mL/min.

To prepare covalently labelled fluorescent lambda DNA for loop extrusion without intercalators (cf. Fif.Sx in SI), we used the Label IT nucleic acid labeling Cy5 kit (Mirus Bio MIR 3725) at 10x diluted dye concentration. Biotin handles were added by ligating primers JT0041 (phospho- GGGCGGCGACCT - Bio) and JT0042 (phospho- AGGTCGCCGCCC -Bio) using T4 DNA ligase in T4 ligase buffer (New England Biolabs), with 1 mM ATP overnight at 16°C. The final linear construct was cleaned-up using an ÄKTA Start (Cytiva), with a homemade gel filtration column containing 46 mL of Sephacryl S-1000 SF gel filtration media, run with TE + 150 mM NaCl buffer at 0.5 mL/min. The labelling reaction was subsequently performed according to the Label IT protocol.

Protein purification and labelling

His6-TEV-4G-ScRap1-1-827 (Rap1 full length) was induced with 0.5 mM isopropyl-β-D-thiogalactoside (IPTG) four hours at 30°C into *E. coli* strain BL21 (DE3) STAR (Invitrogen). All of the subsequent protein purification steps were carried out at 4°C. Cells were harvested, suspended in lysis buffer (50 mM Tris HCl [pH8@4°C], 1M NaCl, 1 mM DTT, 20 mM Imidazole 1 mg/mL lysozyme, 1 mM 4-(2-aminoethyl) benzenesulphonyl fluoride (AEBSF), 10 mM benzaminide, 2 μM pepstatin) and disrupted by sonication. Extract was cleared by centrifugation at 186,000*g* for 1 hour at 4°C and then incubated at 4°C with NiNTA resin (QIAGEN) for 4 h. Mixture was poured into an Econo-Column®Chromatography column (BIO-RAD). After extensive washing of the resin first with buffer A (20 mM Tris HCl [pH8@4°C], 500 mM NaCl, 1 mM DTT, 20 mM Imidazole) and then with buffer B (20 mM Tris HCl [pH8@4°C], 100 mM NaCl, 1 mM DTT, 40 mM Imidazole), protein was eluted with buffer B complemented with 400 mM imidazole. Fractions containing purified His6-TEV-4G-ScRap1-1-827 were pooled and applied to a ResourceQ 1ml column (Cytiva) equilibrated with buffer C (20 mM Tris HCl [pH8@4°C], 100 mM NaCl, 1 mM DTT, 1mM EDTA). Protein was eluted with a 20 mL linear gradient of 0.1–1 M NaCl. Fractions containing the purified protein were pooled and directly applied to a 1 ml HiTrap Heparin HP column (Cytiva) equilibrated with buffer C. A 30 mL linear gradient of 0.1-0.8 M NaCl was performed. TEV protease was added to the pooled fractions containing purified His6-TEV-4G-ScRap1-1-827 and the mixture was directly dialyzed against buffer D (20 mM Tris HCl [pH8@4°C], 150 mM NaCl, 1 mM DTT, 1mM EDTA) at 4°C overnight. The mixture was then incubated with NiNTA resin (QIAGEN) for 2 hours and the purified 4G-ScRap1-1-827 without its His6-TEV tag was recovered into the flow trough. Concentration was determined using Bradford protein assay with BSA as standard. 4G-ScRap1-310-608 (Rap1 DBD) was purified with the same protocol except the HiTrap Heparin HP column which was omitted.

Rap1 protein was subsequently labelled with Janelia Fluor 646 (JF646) using a sortase reaction followed by ÄKTA purification in a MonoQ column against a 1M NaCl gradient. The labelling efficiency of Rap1-JF646 was estimated to be about 70% from the fluorophore and protein concentrations.

S. cerevisiae condensin was purified as described in Ganji et al.[15] Unlike the expression, purification and fluorescent labelling of condensin,[15,84,85] the composition of -URA-TRP dropout medium used for liquid cultures was thus far not described in detail. Briefly, a 5-fold stock of -URA-TRP was prepared with 40 g/l yeast nitrogen base (Difco BD 291940), 18 g/l casamino acids (Difco BD 228830), 500 mg/l leucine (Merck Sigma L8000), 275 mg/l tyrosine (Merck Sigma T3754), and 275 mg/l adenine (Merck Sigma A8626). With the exception of leucine that was filter-sterilized, all components were autoclaved. For one condensin purification,

typically, 0.5 l of preculture was grown on -URA-TRP medium supplemented with 2 g/l D-glucose (Merck Sigma G8270), six liters of main culture on -URA-TRP supplemented with 2 g/l D-raffinose (Biosynth R-1000), and condensin expression was induced with 2 g/l D-galactose (Biosynth G-1700).

Full length Escherichia coli LacI (Uniprot P03023), appended on the C-terminus with a PAGGSPGLEVNKGSGSTSGSGTS-linker, a SNAP®-tag, a HRV-3C protease cleavage site and a His8-tag, was expressed from a pBAD-derived plasmid in Escherichia coli ER2566 cells (New England Biolabs, fhuA2 lacZ::T7 gene1 [lon] ompT gal sulA11 R(mcr73::miniTn10–TetS)2 [dcm] R(zgb-210::Tn10–TetS) endA1 Δ(mcrCmrr)114::IS10). Cells were grown at 37°C in baffled flasks on LB supplemented with 100 μg/ml ampicillin, expression was induced at an OD600 of ∼0.6 with 0.2% (w/v) arabinose, and cells were harvested after three 3 hours expression at 37°C (10 min 4000 rpm, Beckman JLA8.1000 rotor). After washing the cells in PBS (Merck Sigma P4417) they were resuspended in PBS and lysed using a CF1 cell disruptor (Constant Systems) at 20 kpsi, 4°C, and unbroken cells and aggregates were pelleted in a Beckman Ti45 rotor (30 min, 40.000 rpm, 4°C). The clarified lysate was applied to 2 ml Talon Superflow resin (Cytiva 28-9575-02) pre-equilibrated with PBS, and incubated for one hour while rotating at 4°C. Subsequently, the resin was washed with 50 ml PBS supplemented with 20 mM imidazole (Merck Sigma I202) and 500 mM NaCl (Merck Sigma S9888), and finally LacI-SNAP was eluted in 15 ml of PBS supplemented with 200 mM imidazole. Proteins were concentrated using a MWCO 10 kDa Vivaspin 20 centrifugal concentrator (Merck Sigma Z614610), labelled at room temperature for 30 minutes with 100 μM SNAP-Surface Alexa Fluor 647 (New England Biolabs S9136S). Finally, labelled LacI-SNAP was purified by size exclusion chromatography on a Superdex 200 Increase 10/300 column (Cytiva 28990944) pre-equilibrated with 20 mM Tris/HCl pH7.0 (Merck Sigma T1503 & T5941), 100 mM NaCl, 50 μM TCEP (Merck Sigma 646547), eluting at approximately 11 ml.

Single-molecule-visualization assay

For the single-molecule loop extrusion assay, flow cells were prepared as previously reported.[15] Briefly, glass slides and coverslips were cleaned using successive rounds of sonication in acetone and 1M KOH followed by piranha etching. The glass surface was functionalised using aminosalinization and the surface was passivated using mPEG-SVA (Laysan Bio) and $MS(PEG)_4$-NHS-Ester (Laysan Bio) in the presence of biotin-PEG-SVA (Laysan Bio). Before experiments, the flowcell was briefly incubated with streptavidin (MP Biomedicals) in T20 buffer (40 mM tris-HCl pH 8.0, 20 mM NaCl, 0.2 mM EDTA) and with 5 mg/ml BSA (ThermoFisher Scientific) also in T20 buffer. Rap1 was bound to the long linear constructs by incubating at room temperature at a 5-fold excess of protein to binding site for at least 1h in 100 mM KGlu, 2.5 mM $MgCl_2$, 20 mM Tris pH 7.4, 1 mM DTT, 0.25 mg/ml BSA. After incubation, the Rap1-DNA complex was flushed into the flowcell. DNA was visualized by adding 100 nM SytoxOrange (SxO) DNA dye. Unbound complexes were flushed out and the buffer was changed to loop extrusion/imaging buffer (50 mM KGlu, 2.5 mM $MgCl_2$, 40 mM Tris pH 7.5, 2 mM Trolox, 1 mM DTT, 0.25 mg/ml BSA, 5% glucose, 10 nM catalase, 18.75 nM glucose oxidase, 2 mM ATP). Purified yeast condensin was added at 0.5-1 nM in imaging buffer at a flow rate of 0.5 μL/min until loops were observed and the flow was stopped. Imaging was done with a HILO microscope, as previously described,[15] with a red (637 nm, 15 mW) and a green laser (561 nm, 0.2 mW) in alternating light excitation mode.

Rap1-DNA binding validation

Binding efficiency was estimated to be near-100% from fluorophore bleaching in our single-molecule fluorescence visualization assay. To this end, Rap1-JF646 was incubated with linear constructs that contain 2 tandem Rap1 binding sites. After flushing the binding reaction into the flow cell, bleaching was done at 25mW power with the 637 nm laser. Individual fluorescent spots were tracked and their fluorescence plotted as in Figure S5A. The number of observed bleaching steps were counted for 46 spots using a step-finding hidden Markov model (sfHMM).[86] As shown in Figure S5B, half of the traces showed 1 and the other half showed 2 bleaching steps (50 ±14%, N=46). This distribution of bleaching steps is in good accordance with the 70% labelling efficiency, from which we expect to observe 54% of traces with a Rap1-JF646 signal to show two steps if both binding sites are occupied ($E^2/(E^2 + 2E(1-E))$, where E is the labelling efficiency). There is no significant difference between the expected 54% and our observed 50% (p=0.16, one-sided binomial test), indicating a near-100% binding efficiency. Binding specificity was visualized using the binding positions along the DNA molecule from the same bleaching experiment (Figure S5C). The Rap1 binding sites were positioned at roughly 40% along the DNA.

To measure the residence time (Figures S5D–S5G) of Rap1 to its binding site, we used an assay similar to that described above for determining the binding specificity. Briefly, we used a DNA construct with 2 tandem Rap1 binding sites, incubated with Rap1 at a ratio of protein to binding site of 10, for >1h at room temperature. Imaging was performed in the imaging buffer described above without ATP with an oxygen scavenger system to minimize photobleaching (50 mM KGlu, 2.5 mM $MgCl_2$, 40 mM Tris pH 7.5, 2 mM Trolox, 1 mM DTT, 0.25 mg/ml BSA, 5% glucose, 10 nM catalase, 18.75 nM glucose oxidase). The constructs were imaged for 3h with infrequent imaging (1 image per 4s) to reduce photobleaching for this long measurement. Data was analyzed similar to described above, where unbinding events were counted as a downward step in kymographs, and steps were analyzed using sfHMM.[86]

Atomic force microscopy

For AFM imaging, short DNA fragments containing Rap1 binding site arrays were produced. The same Rap1 arrays as for the single-molecule loop extrusion were cut with PvuII (New England Biolabs) and fragments containing Rap1 repeats were separated from the backbone using a similar ÄKTA procedure as mentioned above: ÄKTA Start (Cytiva) with a homemade gel filtration column containing

46 mL of Sephacryl S-1000 SF gel filtration media, run with TE + 150 mM NaCl buffer at 0.5 mL/min. To concentrate the sample, we used the vacufuge plus speedvac (Eppendorf) to reduce the volume. Next, the Rap1 array fragments were dialyzed to water to remove excess salt. Final concentration of DNA fragments was between 1 and 14 nM.

Samples were prepared by mixing DNA at a concentration of 0.5 nM with Rap1 to a protein:binding site ratio of 4.1. We used the same fluorescently labelled full-length Rap1 proteins as in the single-molecule visualization assay. Samples were incubated in a similar buffer as for the single-molecule visualization assay: 100 mM KGlu, 20 mM Tris pH 7.4, 1 mM DTT. Some of the samples had slightly higher ratios of protein to binding site due to a calculation error, but we found no significant effect on the binding in this concentration regime.

For surface deposition and measurement, we prepared mica substrates by punching 3.2 mm mica discs from mica sheets (V4 grade, SPI supplies) and gluing them to magnetic stainless-steel discs with 2-component epoxy glue. The mica discs were cleaved with adhesive tape before each preparation to provide a clean surface. To ensure stable adhesion of the DNA to the mica surface, poly-L-lysine (PLL) was deposited onto the mica at a concentration of 0.01% (w/v), incubated for 3 minutes, washed with pure water and dried in a stream of nitrogen. We found that shorter incubation of the PLL, as well as the use of poly-L-orthinine instead of PLL, would lead to incomplete coverage of the mica, which promoted alignment of parts of the DNA molecules along straight lines separated by angles of 60 degrees, presumably parallel to the crystal axes of the mica. DNA-Rap1 samples were incubated for 45-90 minutes at room temperature (21°C) and then 3 μl drops were deposited onto the PLL-coated mica substrates. After 1 minute, the sample was gently washed using 200 μl of buffer applied and extracted with two separate pipettes. The sample was then placed onto the microscope and imaged in buffer. The microscope was a Bruker Multimode, with NanoScope V controller and version 9.1 Nanoscope software. The imaging mode was PeakForce QNM, with a tapping frequency of 4 kHz and a force setpoint and amplitude manually tuned for optimal image quality, typically 100 pN and 12 nm. Images were acquired with a pixel size of 2 nm, and processed for subtraction of background artifacts using the 'align rows' and 'remove polynomial background' filters in Gwyddion.[87]

QUANTIFICATION AND STATISTICAL ANALYSIS

Analysis of *in vivo* experiments

The statistical analysis and p values for the ChIP-qPCR assay were obtained using unpaired t-test. The statistical analysis and p values for the microscopy-based assay were obtained using the Mann-Whitney test.

Analysis of loop extrusion experiments

Image analysis and quantification was performed as previously.[38] Briefly, all DNA molecules that showed an extruding loop were selected as region of interest for further analysis. All selected regions of interest were subsequently median-filtered to remove the background and analyzed in custom kymograph analysis software.[88] Encounters were manually attributed as passing/blocking depending on the distance between the extruded loop and the Rap1/LacI array, moving MSD of the array after the encounter, and the growth of the loop after the encounter. The MSD is calculated as a 51-frame moving average of the MSD of a tracked object at each frame. DNA tension of a passing/blocking event was calculated using the Marko-Siggia interpolation function using the content of the non-extruded DNA and end-to-end, correcting for the SxO intercalation effects.[35,89] When blocking efficiencies are reported without the mention of a particular DNA tension, it is the overall blocking efficiency regardless of the DNA tension, i.e. the total of all bins.

Details of statistical tests, error bars, and other confidence intervals are given in the respective figure captions.

For the temporary stalling analysis (Figure S6), we analyzed all passing events and estimated the stalling time for each trace from the plateau in loop size before passing the Rap1 array into the loop. To observe this plateau, at least several acquired frames are necessary to discern a decrease in loop size beyond noise, which sets the lower bound for the lower bound for the time resolution to ~1s. Note that these encounters are still overall counted as 'passing' because the array eventually did pass into the loop.

Details of statistical tests, error bars, and other confidence intervals are given in the respective figure captions.

Analysis of AFM experiments

To analyze the contour lengths and array end-to-end lengths, we used a homebuilt Matlab analysis package named DNAcontour. This package in the version that was used to produce the data presented here, is available at https://gitlab.tudelft.nl/allards-matlab-repo/allards-matlab-repo/-/tree/RAP1_paper/DNAcontour. To automatically select DNA molecules from AFM images, we first applied smoothing using a multi-pass Gaussian blur, followed by thresholding and filtering based on a potential DNA molecule's height, size, and aspect ratio. To calculate the trajectories of the DNA molecules, they were skeletonized and resulting branches were connected. The initial guess for trajectories was obtained by connecting the branches with Dijkstra's algorithm and taking the longest shortest path between endpoints. These trajectories were manually corrected where needed and the start- and endpoints of the Rap1 arrays were manually annotated. The obtained trajectories were then iteratively refined by optimizing the trajectories for the local maxima in a smooth curve. The end-to-end lengths were then calculated as the distance between the endpoints of the Rap1 arrays and the contour length was determined from the length of the DNA trajectories as shown in Figure 3D.